Supplementary Information: A catalyst design for selective electrochemical reactions: Direct production of hydrogen peroxide in advanced electrochemical oxidation

Young-Jin Ko [#a], Keunsu Choi [#b], Boram Yang [c], Woong Hee Lee [d], Jun-Yong Kim [a,e], Jae-Woo Choi [c], Keun Hwa Chae [f], Jun Hee Lee [g], Yun Jeong Hwang [d,h], Byoung Koun Min [d,i], Hyung-Suk Oh [d,h*] and Wook-Seong Lee [a*]

[a] Center for Electronic Materials, Korea Institute of Science and Technology, Hwarang-ro 14-gil 5, Seongbuk-gu, Seoul 02792, Republic of Korea

[b] Department of Physics, Ulsan National Institute of Science and Technology, UNIST-gil, Ulsan 44919, Republic of Korea

[c] Center for Water Resource Cycle Research, Korea Institute of Science and Technology, Hwarang-ro 14-gil 5, Seongbuk-gu, Seoul 02792, Republic of Korea

[d] Clean Energy Research Center, Korea Institute of Science and Technology, Hwarang-ro 14-gil 5, Seongbuk-gu, Seoul 02792, Republic of Korea

[e] Department of Materials Science and Engineering, Korea University, Seoul, 02841, Republic of Korea

[f] Advanced Analysis Center, Korea Institute of Science and Technology, Hwarang-ro 14-gil 5, Seongbuk-gu, Seoul 02792, Republic of Korea

[g] School of Energy and Chemical Engineering, Ulsan National Institute of Science and Technology, UNIST-gil, Ulsan 44919, Republic of Korea

[h] Division of Energy and Environmental Technology, KIST School, Korea University of Science and Technology, Seoul 02792, Republic of Korea

[i] Green School, Korea University, 145 Anam-ro, Seongbuk-gu, Seoul 02841, Republic of Korea

[#]These authors contributed equally.

***Corresponding authors**
E-mail addresses: hyung-suk.oh@kist.re.kr (H.-S. Oh), wslee@kist.re.kr (W.-S. Lee)

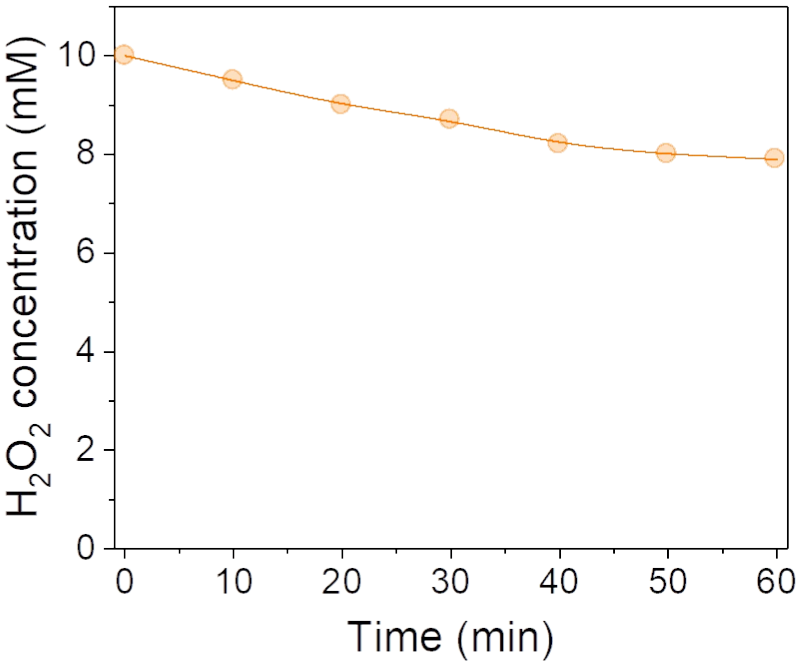

Fig. S1. The H_2O_2 concentration vs time profile. The H_2O_2 decomposed by peroxide disproportionation reaction (PDR, H_2O_2 (aq) → H_2O (l) + $0.5O_2$ (g)). As shown in Fig. S1, approximately 20% of H_2O_2 decomposed in 2 hours.

Table S1. The compositions of the synthesized catalyst samples.

Sample	Mass ratio by ICP (wt%)		Atomic ratio by XPS (%)	
	Pt	Ag	Pt	Ag
Pt/C	39.6	0	4.1	0
Pt_3Ag_1	9.7	3.6	1.12	0.24
Pt_2Ag_1	9.8	2.4	0.89	0.38
Pt_1Ag_1	9.8	5.3	0.72	0.73
Pt_1Ag_2	9.1	10.1	0.68	1.41

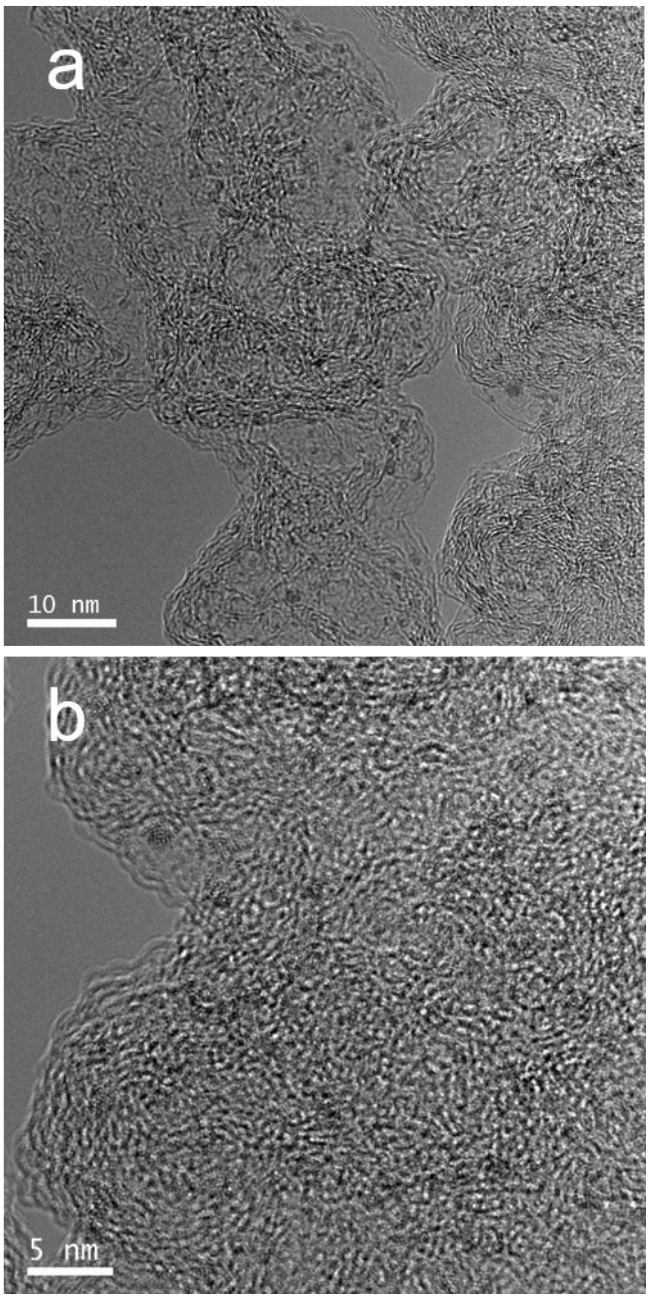

Fig. S2. The HR-TEM images of Pt_1Ag_1/C catalyst. (**a**) Low- and (**b**) high-magnification. The images indicate the presence of ca. 1 ~ 2 nm Pt－Ag alloy clusters in the catalyst.

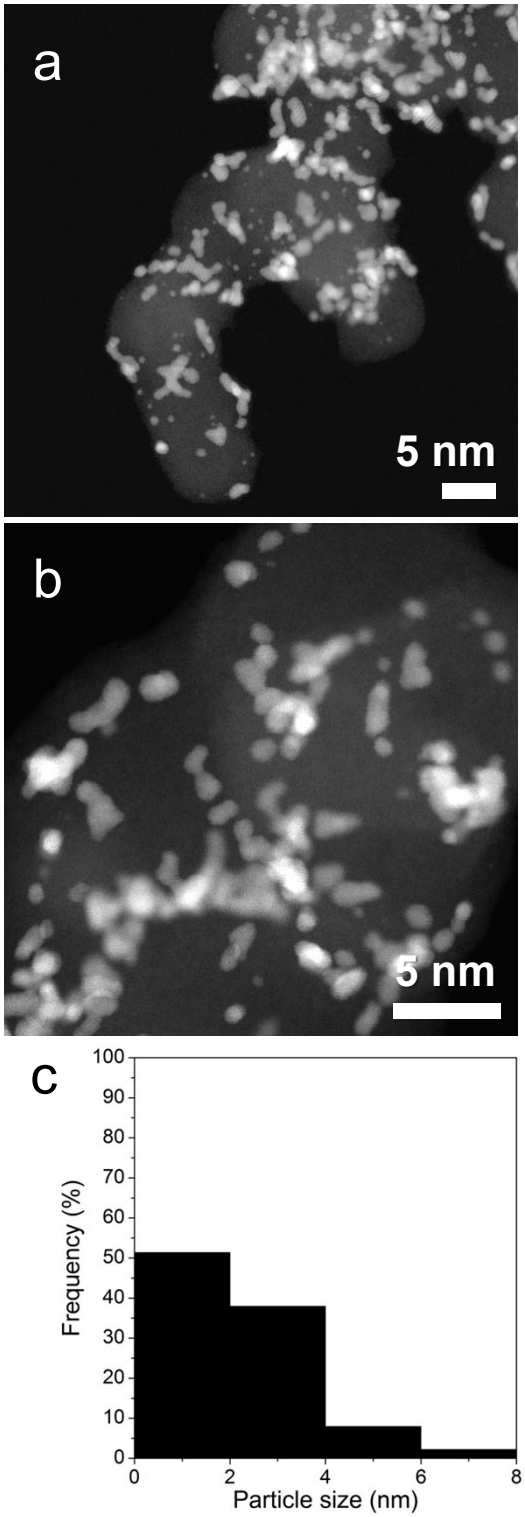

Fig. S3. HR-STEM images and the particle size distribution of Pt/C catalyst. (**a-b**) To visualize the dispersion and structure of Pt species, atomic resolution HAADF-STEM images were overlapped on the HR-STEM image of Pt/C; scale bar, 5 nm. (**c**) Histograms of the particle size distributions for Pt/C. Average Pt particle size of Pt/C was fitted with a Gaussian function.

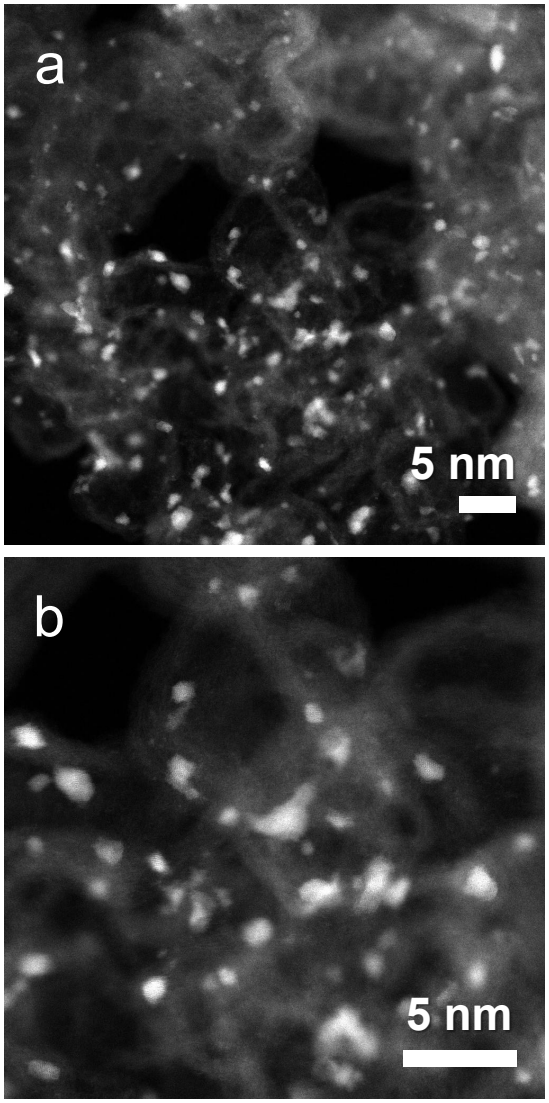

Fig. S4. HR-STEM images of Ag/C catalyst. (**a**) Low- and (**b**) high-magnification to visualize the dispersion and structure of Pt species, atomic resolution HAADF-STEM images were overlapped on the HR-STEM image of Pt/C; scale bar, 5nm.

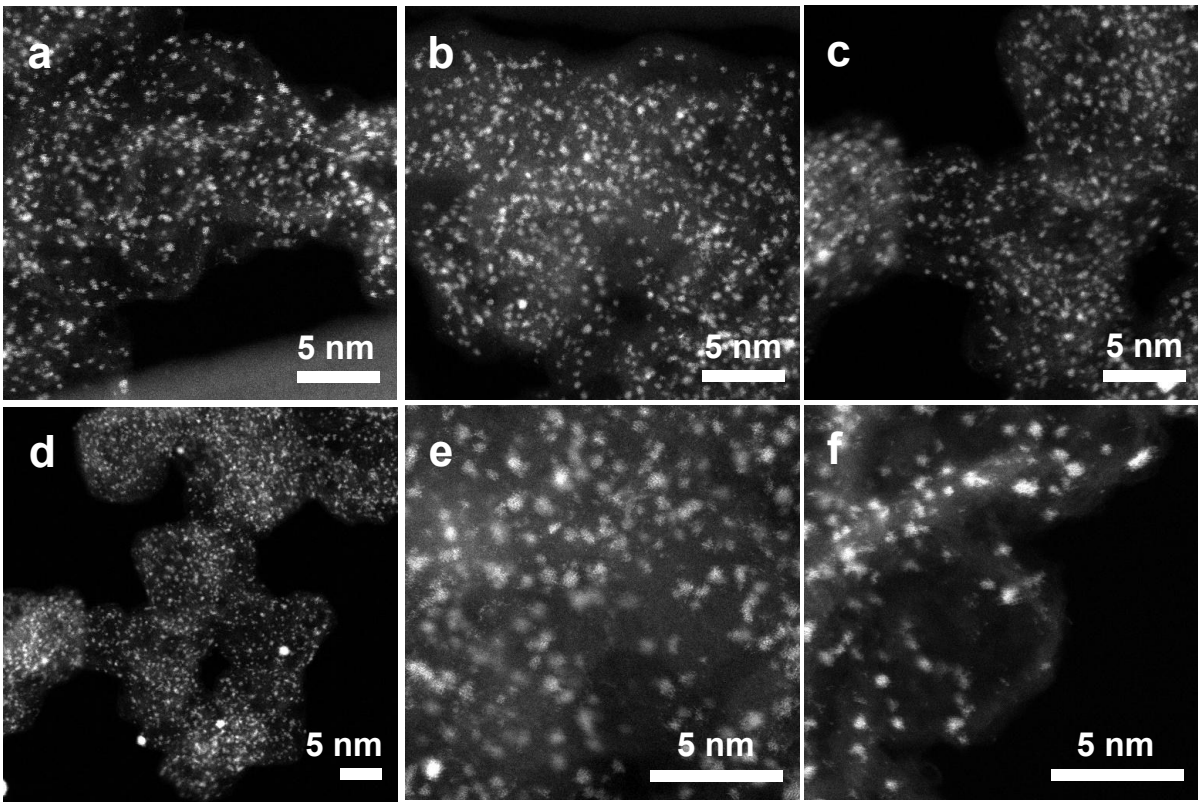

Fig. S5. The additional HR-STEM images of Pt_1Ag_1/C catalyst with different magnifications (all scale bars are 5 nm). (**a-f**) the images taken at different spots indicated the prevailing sub-nanometer scale Pt−Ag particles. In general, sub-nanometer scale metal particles become unstable to undergo the extensive agglomeration under the high energy electron beam (over 200 kV) [1, 2]. By contrast, the present Pt−Ag alloy particles were highly resistant against the agglomeration; the thermal vibrations and occasional atomic hopping were the only activities observed under the electron beam of 300 kV (see Movie S1).

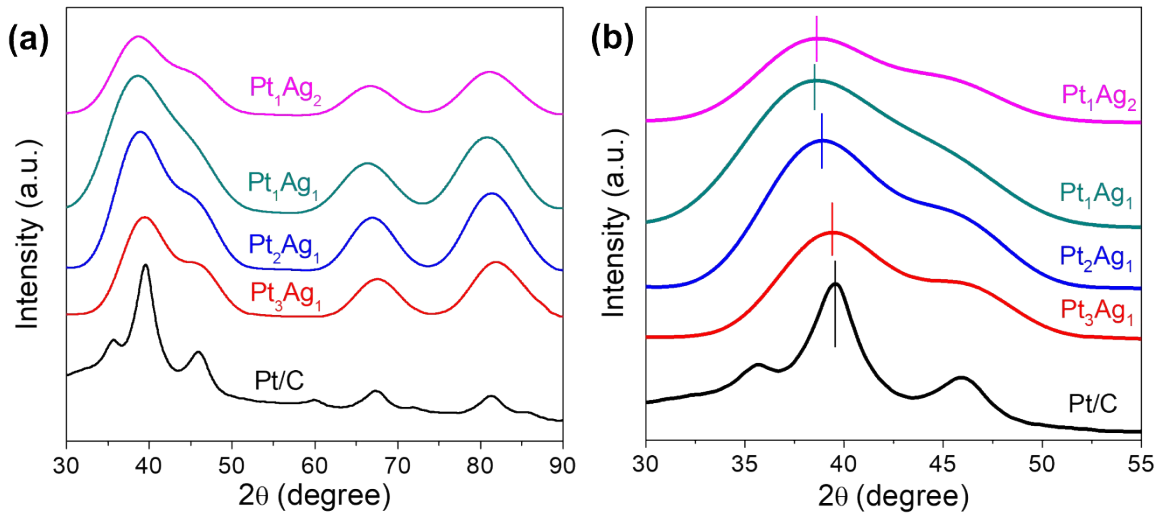

Fig. S6. (a) Wide-angle XRD patterns of Pt/C and Pt-Ag alloy catalysts. (b) The Pt(111) and (200) planes were observed. The peak shift of Pt-Ag alloy catalysts was increased with degree of Pt-Ag coupling. The peaks of Pt-Ag alloy catalysts are broad, and the particle sizes calculated by Bragg's law are Pt_3Ag_1: 1.4 nm, Pt_2Ag_1: 1.28 nm, Pt_1Ag_1: 1.16 nm, Pt_1Ag_2: 1.21 nm, respectively.

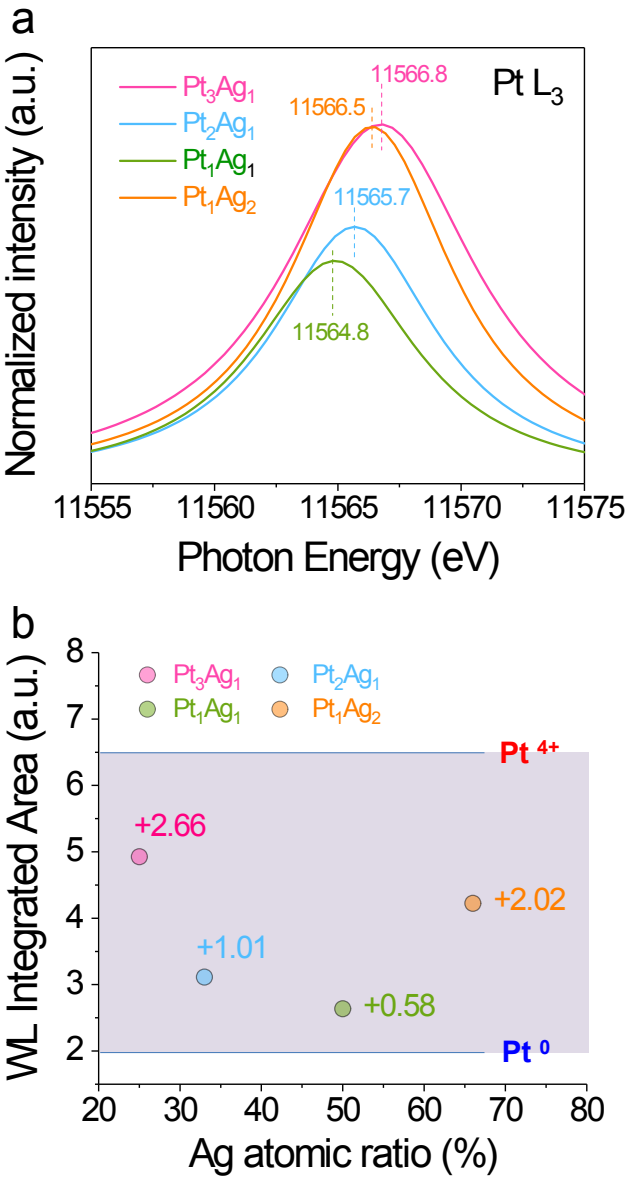

Fig. S7. The oxidation state of Pt−Ag alloy catalysts. (**a**) The white-line positions of Pt−Ag alloy catalysts and (**b**) the oxidation states vs. Ag ratio profile: The XANES analysis was carried out using arctangent and Lorentzian functions to fit the white-line position. The white-line area intensities were found to be 2.0 and 6.6, which agreed with those of Pt^0 and Pt^{4+}, respectively, as reported by H.Yoshida *et al* [3].

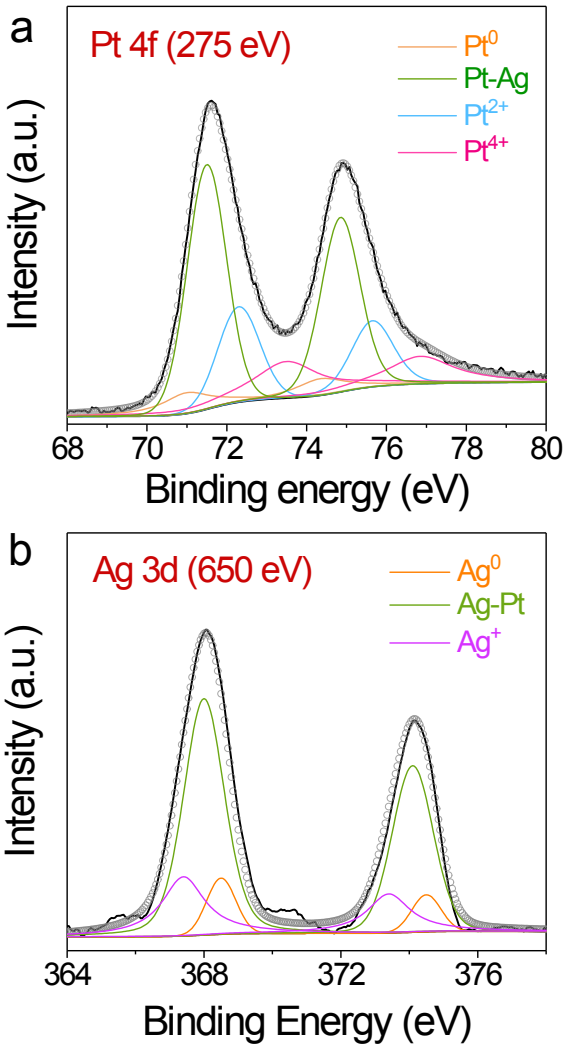

Fig. S8. Top-surface structure of Pt_1Ag_1 catalyst. (**a**) Pt 4f and (**b**) Ag 3d PES spectra of Pt_1Ag_1/C catalyst: for the measurement of top-surface, the input energies were 275 eV (Pt) and 650 eV (Ag), respectively.

Table S2. EXAFS fitting results of Pt−Ag alloy catalysts. The multi-shell fitting results (Δk = 2 ~ 12 Å^{-1}) of the experimental EXAFS spectrum

Sample		Coordination number (CN)	R (Å)	$\Delta\sigma^2$ (Å^2)	ΔE_0 (eV)	Short-range order (η)
Pt_3Ag_1	Pt–Pt	4.90 ± 0.80	2.68 ± 0.008	0.0065 ± 0.001	8.0 ± 1.50	0.73
	Pt–Ag	0.45 ± 0.30	2.82 ± 0.010	0.0007 ± 0.004		
	Pt–C (O)	1.40 ± 0.11	2.03 ± 0.003	0.015 ± 0.006		
Pt_2Ag_1	Pt–Pt	3.68 ± 0.46	2.69 ± 0.009	0.0065 ± 0.001	9.0 ± 0.01	0.69
	Pt–Ag	0.49 ± 0.20	2.93 ± 0.003	0.0007 ± 0.004		
	Pt–C (O)	0.67 ± 0.30	2.05 ± 0.028	0.015 ± 0.006		
Pt_1Ag_1	Pt–Pt	0.54 ± 0.035	2.54 ± 0.029	0.0052 ± 0.004	7.2 ± 0.90	–0.70
	Pt–Ag	3.72 ± 0.40	2.95 ± 0.013	0.0124 ± 0.0016		
	Pt–C (O)	0.1 ± 0.02	1.98 ± 0.017	0.0164 ± 0.0017		
Pt_1Ag_2	Pt–Pt	0.30 ± 0.26	2.52 ± 0.026	0.0031 ± 0.004	7.7 ± 0.84	–0.15
	Pt–Ag	3.27 ± 0.38	2.90 ± 0.010	0.0132 ± 0.0016		
	Pt–C (O)	0.67 ± 0. 24	1.95 ± 0.016	0.0409 ± 0.0092		

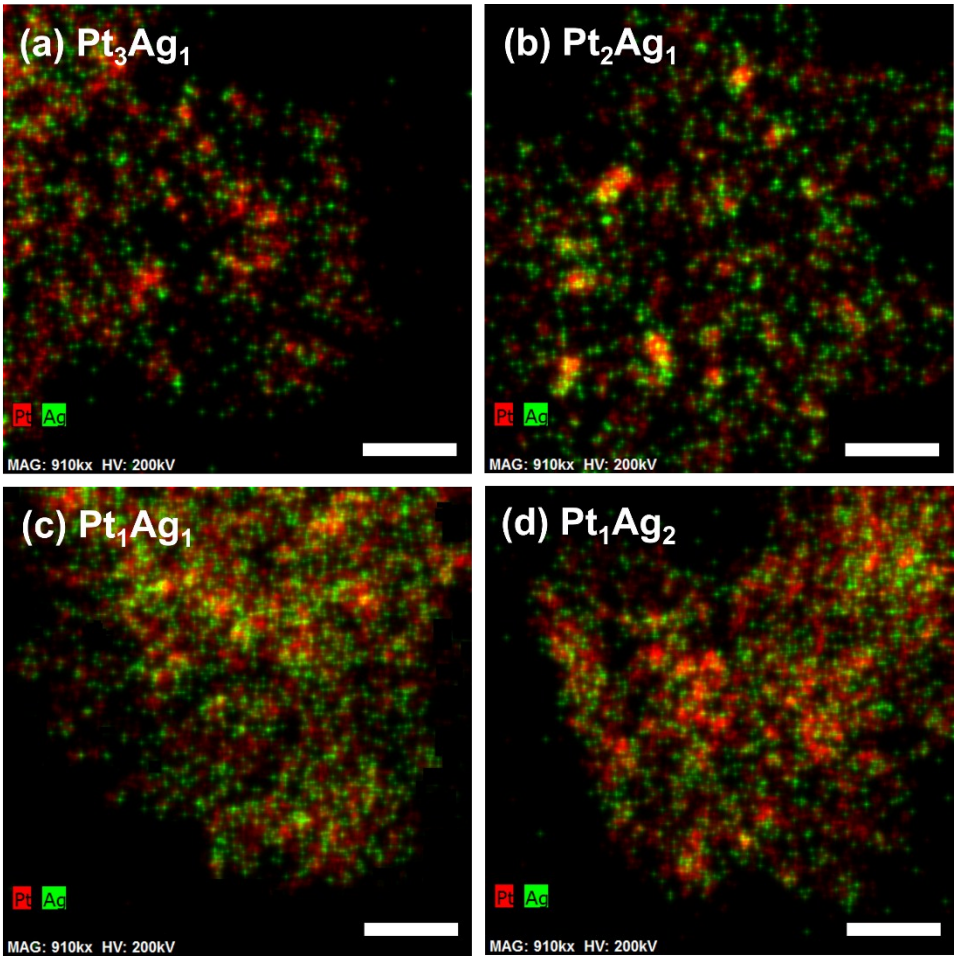

Fig. S9. EDS mapping images of the Pt-Ag alloy catalysts. The scale bars are 5 nm and the measurement time was 10 minutes.

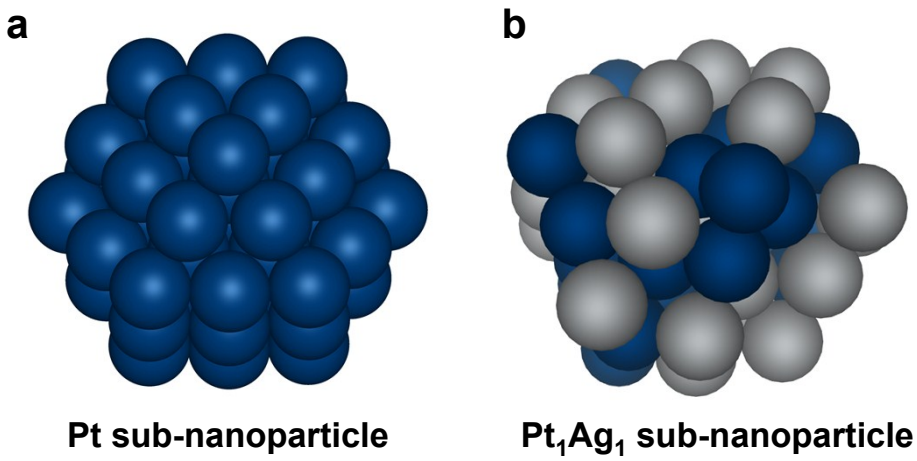

Fig. S10. The model structures of (**a**) Pt sub-nanoparticle and (**b**) Pt–Ag alloy sub-nanoparticle. Considering the particle size (~ 1.5 nm) measured in the experiment, we built the nanoparticle with 55 atoms.

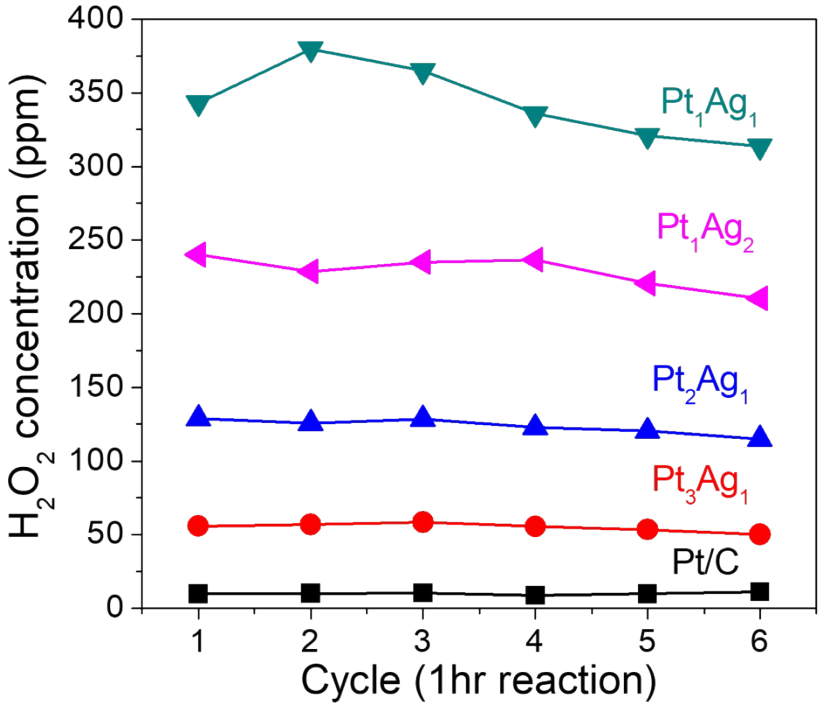

Fig. S11. Accumulated concentrations of H_2O_2 produced on the Pt/C and Pt-Ag alloy catalysts with the OER counter reaction during repeated 1-hour operation cycles.

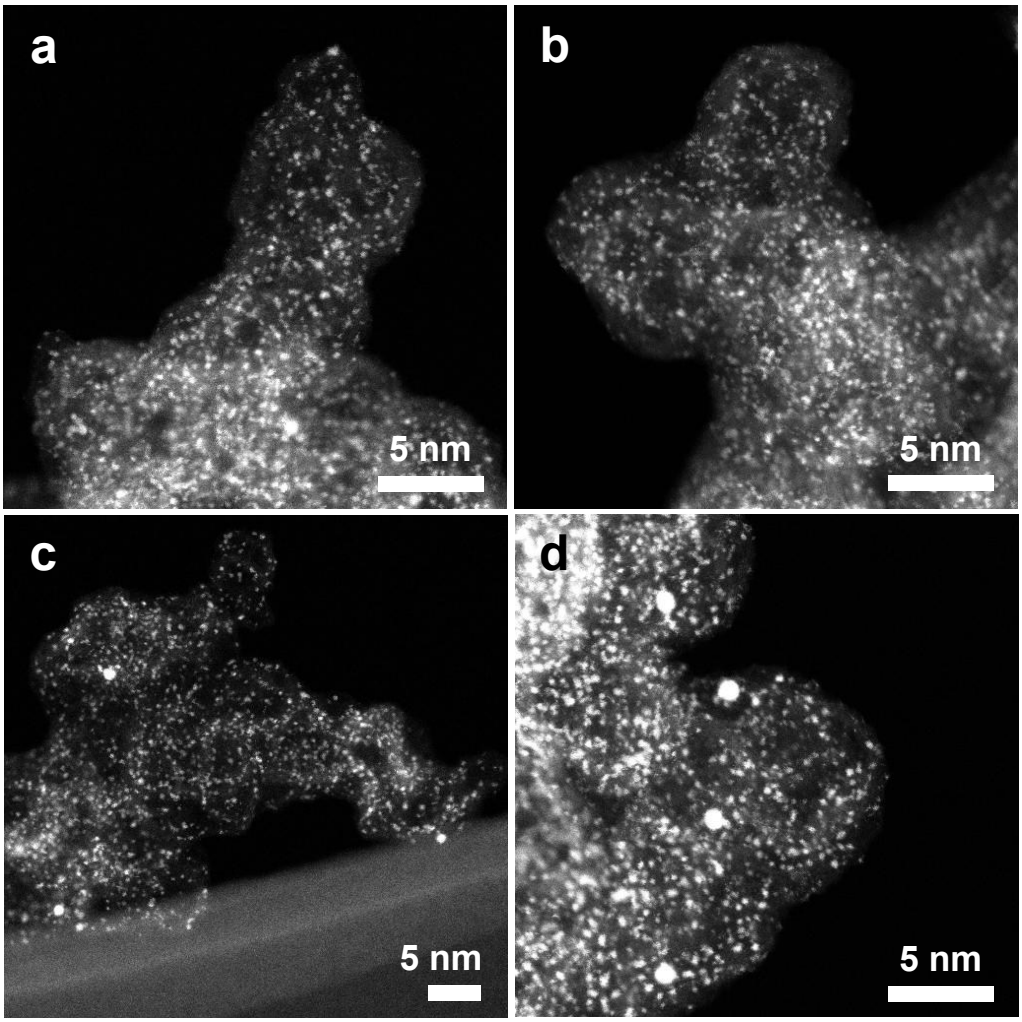

Fig. S12. HR-STEM images of Pt_1Ag_1/C catalyst after repeated H-Cell operation with different magnifications (all scale bars are 5 nm). (**a-d**) After 6 cycles of 1 hr operations, HR-STEM images were taken at the acceleration voltage of 300 kV. The result indicated that the number of sub-nanoparticles only slightly increased, while the majority of the particles retained their sizes.

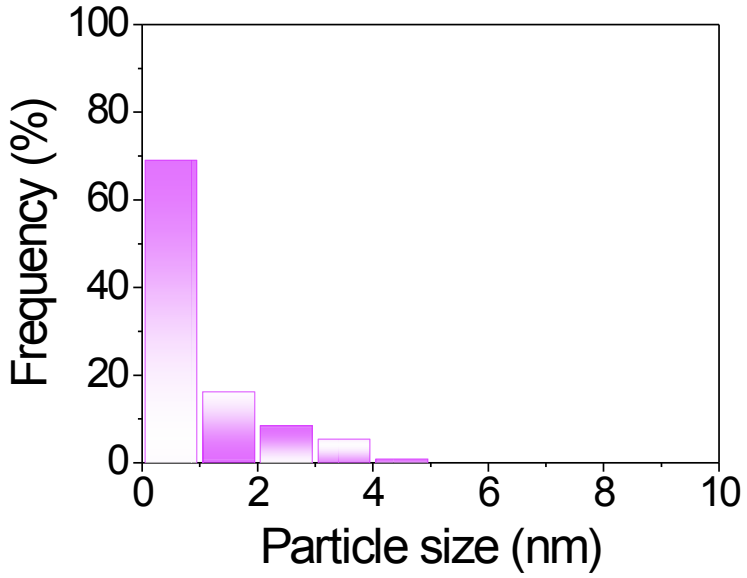

Fig. S13. Particle size distribution of Pt_1Ag_1/C after 6 cycles of 1 hr operations from HR-STEM images (Fig. S12).

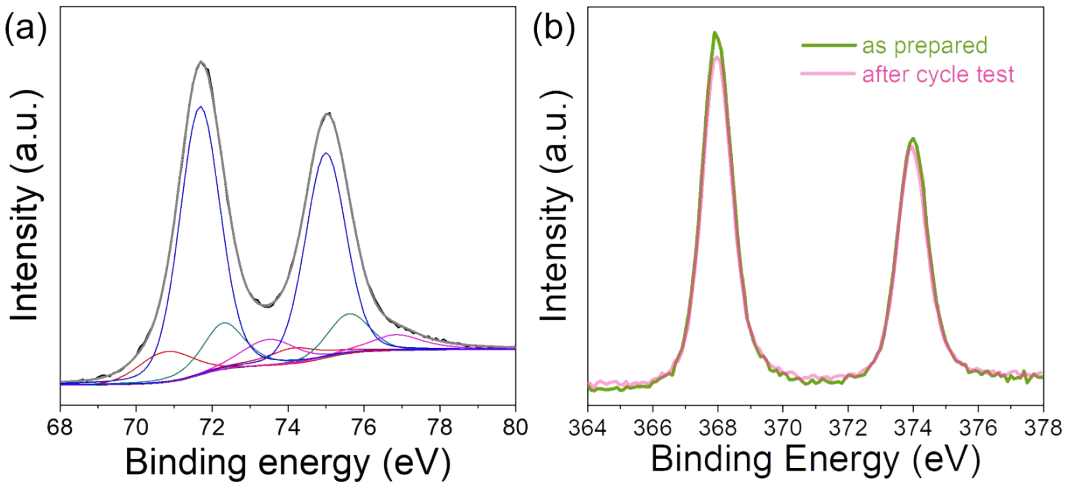

Fig. S14. The XPS spectra of Pt_1Ag_1 catalyst after 6 cycles of 1 hr operations for (a) Pt_{4f} and (b) Ag_{3d}. XPS-Pt4f spectra were deconvoluted with Pt^0 (redline), Pt^{2+} (dark-cyan lines), Pt^{4+} (magenta lines), and Pt−Ag (blue lines) phases. The $Pt^0/Pt^{2+}/Pt^{4+}$/Pt−Ag ratios change from 11.5/7.7/3.8/77.0 to 9.3/13.8/8.8/68.0, respectively.

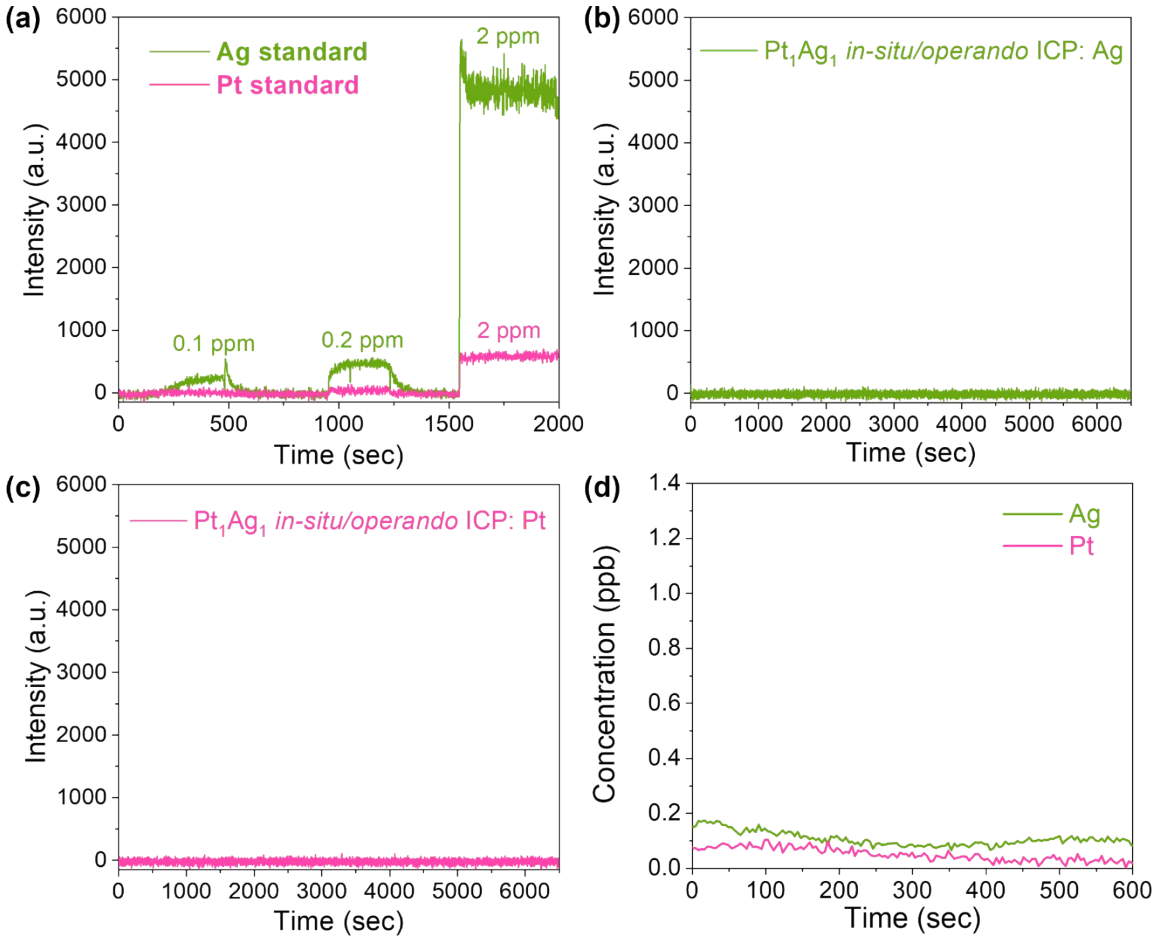

Fig. S15. The time-plasma intensity profiles of Ag and Pt obtained by in-situ ICP-OES. (a) Ag and Pt standard profiles, (b) Ag and (c) Pt dissolution profiles for Pt_1Ag_1 catalyst. The *in-situ/operando* ICP-OES measurements for Pt_1Ag_1 catalyst were performed under 0.2 V vs RHE at room temperature. (d) The time-plasma intensity profiles of Ag and Pt obtained by in-situ ICP-MS for Pt_1Ag_1 catalyst. The *in-situ/operando* ICP-MS measurements were also performed under 0.2 V vs RHE at room temperature.

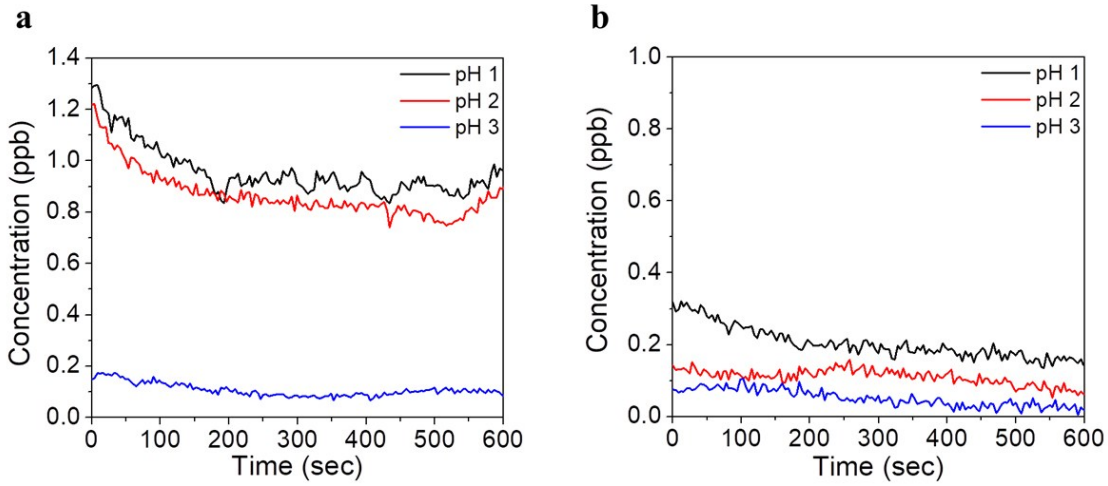

Fig. S16. The time-plasma intensity profiles of (a) Ag and (b) Pt from pH 1 to pH 3 obtained by *in-situ/operando* ICP-MS for Pt_1Ag_1 catalyst. The *in-situ/operando* ICP-MS measurements were also performed under 0.2 V vs RHE at room temperature.

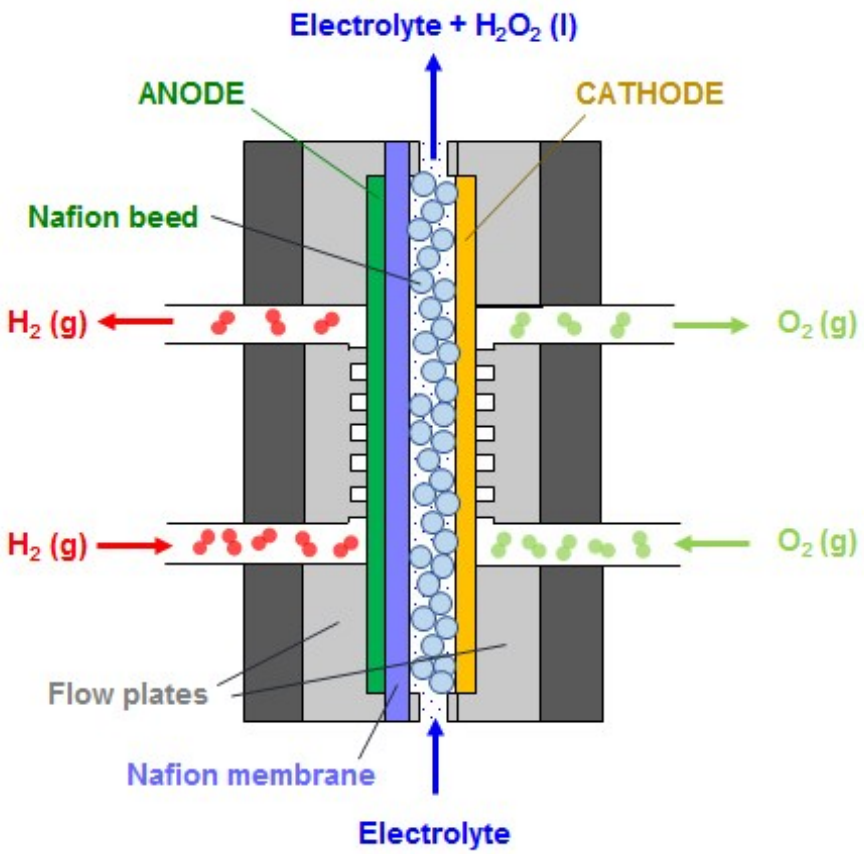

Fig. S17. Cross-sectional schematic diagram of renovated single-cell for ORR. Pt/C catalyst was deposited on the gas diffusion layer (GDL) as an anode. Nafion membrane was located between the anode and cathode, which was assembled between the two flow plates. The H_2 gas and the O_2 gas were supplied to the anode and the cathode, respectively. In order to increase the diffusion of produced H_2O_2, the electrolyte solution was supplied to flow between the Nafion membrane and the cathode. Nafion beads were applied in the channel to mediate the proton diffusion.

Table S3. Performance comparison of reported various electrocatalysts for H_2O_2 production.

Catalyst		RRDE			H-cell				Single-cell			Ref.
		Electrolyte	**Loading (mg/cm^2)**	**F.E. (%) @ 0.2 V**	**Electrolyte**	**Loading (mg/cm^2)**	**H_2O_2 accumulation**	**F.E. (%)**	**Loading**	**H_2O_2 accumulation**	**F.E. (%)**	
Noble metal catalysts	Pt–Ag/C	0.05 M Na_2SO_4 (pH 3)	0.08	65.4	0.05 M Na_2SO_4 (pH 3)	1 mg/cm^2 (total = 1 mg)	51.5 μmol in 60 min (343 mol/kg_{cat})	69.4	1 mg/cm^2 (total = 10 mg)	514 μmol in 60 min	75.5	This work
							70.9 μmol in 120 min (472 mol/kg_{cat})	67.1		1019 μmol in 120 min	77.3	
	Pt–Hg/C (Pt_1Hg_4 polycrystal)	0.1 M $HClO_4$	0.014	83.3	0.1 M $HClO_4$	-	7.0 μmol in 18.3 min	66.4	0.1 mg/cm^2 (total = not mentioned)	-	Negligible	4, 5
	Ag/C	0.1 M $HClO_4$	0.02	60	0.1 M $HClO_4$	0.1 mg/cm^2 (total = not mentioned)	-	75	0.1 mg/cm^2 (total = not mentioned)	-	30	4
	C–coated Pt	1 M $HClO_4$	0.08	34	-	-	-	-	-	-	-	6
Carbon based materials	N–doped carbon	0.5 M H_2SO_4	0.05	97.1	0.5 M H_2SO_4	0.05 mg/cm^2 (total = not mentioned)	159.9 mol/kg_{cat} in 60 min	72.5	-	-	-	7
	Anthraquinone/ carbon black	0.1 M H_2SO_4	4	89.5	0.1 M H_2SO_4	-	0.74 mol/kg_{cat} in 60 min	26.3	-	-	-	8
	Oxidized-CNT	0.1 M $HClO_4$	0.1	≈ 30	-	-	-	-	-	-	-	9
	F-mrGO (600)**	0.1 M KOH	0.01		0.1 M KOH	0.01 mg/cm^2 (total = 0.005 mg)	-	-	-	-	-	10
Single-atom catalysts	Pt–S	0.1 M $HClO_4$	0.05	94.8	1 M $HClO_4$	2 mg/cm^2 (total = 8 mg)	12.2 mol/kg_{cat} in 60 min	-	-	-	-	11
	Pd–Au	0.1 M $HClO_4$	0.125	85	-	-	-	-	-	-	-	12
	Pt/TiN	0.1 M $HClO_4$	0.015*	76	-	-	-	-	-	-	-	13
	Pt/CuS_x	0.1 M $HClO_4$	0.1	≈ 90	0.5 M $HClO_4$	-	546 mol/kg_{cat} in 60 min	90	-	-	-	14
	Fe-N-C**	0.1 M KOH	0.1	≈ 85	-	-	-	-	-	-	-	15
Non-noble metal catalysts	CoS_2	0.05 M H_2SO_4	0.305	≈ 70	0.05 M H_2SO_4	0.374 mg/cm^2 (total = 0.412 mg)	5.72 μmol in 20 min	54.6	-	-	-	16
							13.08 μmol in 60 min	41.2				
	Co–C	0.1 M $HClO_4$	0.6	95	0.05 M H_2SO_4	1 mg/cm^2 (total = not mentioned)	5 mol/kg_{cat} in 60 min	80	-	-	-	17

* Geometric area is not mentioned.

** Only tested in alkaline condition

References

1. A. Uzun, V. Ortalan, Y. L. Hao, N. D. Browning and B. C. Gates, *Acs Nano*, 2009, **3**, 3691-3695.
2. A. Uzun, V. Ortalan, N. D. Browning and B. C. Gates, *J Catal*, 2010, **269**, 318-328.
3. H. Yoshida, S. Nonoyama, Y. Yazawa and T. Hattori, *Phys Scripta*, 2005, **T115**, 813-815.
4. S. Yang, A. Verdaguer-Casadevall, L. Arnarson, L. Silvio, V. Colic, R. Frydendal, J. Rossmeisl, I. Chorkendorff and I. E. L. Stephens, *Acs Catal*, 2018, **8**, 4064-4081.
5. S. Siahrostami, A. Verdaguer-Casadevall, M. Karamad, D. Deiana, P. Malacrida, B. Wickman, M. Escudero-Escribano, E. A. Paoli, R. Frydendal, T. W. Hansen, I. Chorkendorff, I. E. L. Stephens and J. Rossmeisl, *Nat Mater*, 2013, **12**, 1137-1143.
6. C. H. Choi, H. C. Kwon, S. Yook, H. Shin, H. Kim and M. Choi, *J Phys Chem C*, 2014, **118**, 30063-30070.
7. Y. Y. Sun, I. Sinev, W. Ju, A. Bergmann, S. Dresp, S. Kuhl, C. Spori, H. Schmies, H. Wang, D. Bernsmeier, B. Paul, R. Schmack, R. Kraehnert, B. Roldan Cuenya and P. Strasser, *Acs Catal*, 2018, **8**, 2844-2856.
8. R. B. Valim, R. M. Reis, P. S. Castro, A. S. Lima, R. S. Rocha, M. Bertotti and M. R. V. Lanza, *Carbon*, 2013, **61**, 236-244.
9. Z. Y. Lu, G. X. Chen, S. Siahrostami, Z. H. Chen, K. Liu, J. Xie, L. Liao, T. Wu, D. C. Lin, Y. Y. Liu, T. F. Jaramillo, J. K. Norskov and Y. Cui, *Nat Catal*, 2018, **1**, 156-162.
10. H. W. Kim, M. B. Ross, N. Kornienko, L. Zhang, J. H. Guo, P. D. Yang and B. D. McCloskey, *Nat Catal*, 2018, **1**, 282-290.
11. C. H. Choi, M. Kim, H. C. Kwon, S. J. Cho, S. Yun, H. T. Kim, K. J. J. Mayrhofer, H. Kim and M. Choi, *Nat Commun*, 2016, **7**.
12. J. S. Jirkovsky, I. Panas, E. Ahlberg, M. Halasa, S. Romani and D. J. Schiffrin, *J Am Chem Soc*, 2011, **133**, 19432-19441.
13. S. Yang, J. Kim, Y. J. Tak, A. Soon and H. Lee, *Angew Chem Int Edit*, 2016, **55**, 2058-2062.
14. R. Shen, W. Chen, Q. Peng, S. Lu, L. Zheng, X. Cao, Y. Wang, W. Zhu, J. Zhang, Z. Zhuang, C. Chen, D. Wang and Y. Li, *Chem*, 2019, **5**, 2099-2110.
15. K. Jiang, S. Back, A. J. Akey, C. Xia, Y. Hu, W. Liang, D. Schaak, E. Stavitski, J. K. Nørskov, S. Siahrostami and H. Wang, *Nat Commun*, 2019, **10**, 3997.
16. H. Sheng, E. D. Hermes, X. Yang, D. Ying, A. N. Janes, W. Li, J. R. Schmidt and S. Jin, *Acs Catal*, 2019, 8433-8442.
17. A. Bonakdarpour, D. Esau, H. Cheng, A. Wang, E. Gyenge and D. P. Wilkinson, *Electrochimica Acta*, 2011, **56**, 9074-9081.